Journal of Contaminant Hydrology, 5 (1990) 349–374
Elsevier Science Publishers B.V., Amsterdam — Printed in the Netherlands

MODELING MULTICOMPONENT ORGANIC CHEMICAL TRANSPORT IN THREE-FLUID-PHASE POROUS MEDIA

J.J. KALUARACHCHI and J.C. PARKER

Center for Environmental and Hazardous Materials Studies, Virginia Polytechnic Institute and State University, Blacksburg, VA 24061 (U.S.A.)

(Received September 12, 1989; revised and accepted December 14, 1989)

ABSTRACT

Kaluarachchi, J.J. and Parker, J.C., 1990. Modeling multicomponent organic chemical transport in three-fluid-phase porous media. *J. Contam. Hydrol.*, 5: 349–374.

A two-dimensional finite-element model was developed to predict coupled transient flow and multicomponent transport of organic chemicals which can partition between nonaqueous phase liquid, water, gas and solid phases in porous media under the assumption of local chemical equilibrium. Gas-phase pressure gradients are assumed negligible and liquid flow equations are solved simultaneously using an upstream weighted solution method with time-lagged interphase mass-transfer terms and phase densities. Phase-summed component transport equations are solved serially after computation of the velocity field also by an upstream weighted finite-element method. Mass-transfer rates are evaluated from individual phase transport equations by back-substitution and corrected for mass-balance errors. A number of hypothetical one- and two-dimensional simulations were performed to evaluate the applicability of the model to predict the transport of slightly soluble and volatile organics in three-fluid-phase porous media. Results indicate that mass-transfer rate and fluid density updating have negligible effects during periods of highly transient nonaqueous liquid phase migration but become important for long-term simulations as cumulative dissolution to the water phase and volatilization to the gas phase account for larger proportions of the total mass. Due to low solubilities of environmentally important organic liquids, the efficiency of organic removal by aqueous-phase dissolution and transport can be very slow. Gas-phase diffusion can have a significant influence on the mass transport of organics with large Henry's constants.

INTRODUCTION

Contamination of groundwater resources due to spills or leakage of nonaqueous-phase organic liquids is of great environmental concern due to the hazardous nature of the constituent chemicals. Compositions of fuels, mixed solvent wastes and other organic liquids that find their way into the subsurface are frequently chemically complex. Models for the movement of such materials in soils and groundwater must account for convective and dispersive transport and mass partitioning of multiple species in aqueous, gaseous and nonaqueous liquid phases.

A number of researchers have recently addressed the problem of modeling

0169-7722/90/$03.50

liquid-phase flow in air–oil–water porous media systems in vertical sections (Abriola, 1984; Faust, 1985; Osborne and Sykes, 1986; Kuppusamy et al., 1987; Kaluarachchi and Parker, 1989). Vertically integrated multiphase flow models for areal analysis of organic liquid migration and recovery have also been presented (Hochmuth and Sunada, 1985; Parker et al., 1988; Kaluarachchi et al., 1990; Parker and Lenhard, 1990). Abriola and Pinder (1985) presented a model for multiphase flow and transport of a single partitionable component using a fully coupled simultaneous solution method which proved very computationally intensive. Reeves and Abriola (1988) reported a decoupled solution approach with improved computational efficiency. A compositional model was described by Corapcioglu and Baehr (1987) for multicomponent multiphase organic chemical transport under conditions of steady water flow with immobile oil and air phases and with oxygen-limited biodegradation of organic components. A three-dimensional finite-element model for three-phase flow and multicomponent transport has been developed by Falta and Javandel (1987) which considers nonequilibrium phase partitioning. Sleep and Sykes (1989) discussed a two-dimensional two-phase air–water flow and transport model with oil phase at residual saturation which also considers nonequilibrium interphase transfer.

In this paper, we extend the multiphase flow model of Kaluarachchi and Parker (1989) to include multicomponent constituent transport. Emphasis is placed on the development of computationally efficient and robust algorithms to handle coupling between flow and transport equations. Effects of interphase mass transfer and of transport in aqueous and gaseous phases on organic contaminant behavior in the subsurface will be investigated by means of a number of hypothetical one- and two-dimensional simulations.

MODEL DEVELOPMENT

Multiphase fluid flow

To consider fluid movement in three-fluid-phase air–oil–water systems, mass conservation and flux equations must in general be considered for each mobile phase. Assuming an incompressible porous medium, the p-phase continuity relations may be written in summation notation as:

$$\Phi(\partial \rho_p S_p/\partial t) = -\partial \rho_p q_{p_i}/\partial x_i + R_p \tag{1}$$

where Φ is the medium porosity; ρ_p is the phase density [$\mathrm{M\,L^{-3}}$]; S_p is the fraction of the pore space containing phase p (p-phase saturation); q_{p_i} is the volume flux density of fluid phase p in the i-direction [$\mathrm{L^3\,L^{-2}\,T^{-1}}$]; x_i is the i-direction spatial coordinate; and R_p is the net transfer of mass to (+) or from (−) phase p via contiguous phases per porous medium volume [$\mathrm{M\,L^{-3}\,T^{-1}}$].

The volumetric flux of phase p is described by Darcy's law which may be written in Cartesian tensor notation as:

$$q_{p_i} = (-k_{rp} K_{\mathrm{sw}_{ij}}/\eta_{rp})[\partial h_p/\partial x_j + \rho_{rp} e_j] \tag{2}$$

where i and j are direction indices ($i, j = 1, 2, 3$) with repeated values indicating summation; x_i (or x_j) is the i-th (or j-th) Cartesian coordinate; k_{rp} is the relative permeability to phase p [L^0] which varies from 0 when no p-phase is present to 1 when the medium is saturated with p-phase; $K_{sw_{ij}}$ is the saturated water conductivity tensor; η_{rp} is the ratio of absolute viscosity of phase p to that of uncontaminated water; h_p is the pressure head of phase p expressed in equivalent height of pure water; ρ_{rp} is the ratio of p-phase density to that of uncontaminated water; and e_j ($= \partial z/\partial x_j$) is the j-component of a unit gravitational vector where z is elevation.

Combining eqs. 1 and 2 yields the p-phase flow equation:

$$\Phi \frac{\partial \rho_p S_p}{\partial t} = \frac{\partial}{\partial x_i} \frac{\rho_p k_{rp} K_{sw_{ij}}}{\eta_p} \left[\frac{\partial h_p}{\partial x_j} + \rho_{rp} e_j \right] + R_p \tag{3}$$

We consider the specific case of a three-fluid-phase system with water (p = w), nonaqueous-phase organic liquid or "oil" (p = o) and air (p = a). Gas-phase pressure gradients are assumed to be negligible, allowing solution of water- and oil-phase flow equations without regard to the gas-phase equation. Liquid phases will be assumed incompressible so that phase densities are independent of phase pressures. Changes in fluid density with phase composition will be considered; however, at any given time step the magnitude of $\Phi S_p \cdot \partial \rho_p / \partial t$ will be assumed to have a negligible effect on the flow equation solution. Under these conditions, the flow model reduces to the system of coupled equations:

$$\Phi \rho_w \frac{\partial S_w}{\partial t} = \frac{\partial}{\partial x_i} \frac{\rho_w k_{rw} K_{sw_{ij}}}{\eta_w} \left[\frac{\partial h_w}{\partial x_j} + \rho_{rw} e_j \right] + R_w \tag{4a}$$

$$\Phi \rho_o \frac{\partial S_o}{\partial t} = \frac{\partial}{\partial x_i} \frac{\rho_o k_{ro} K_{sw_{ij}}}{\eta_o} \left[\frac{\partial h_o}{\partial x_j} + \rho_{ro} e_j \right] + R_o \tag{4b}$$

The constitutive model of Parker et al. (1987) is assumed to describe the nonlinear relationship between fluid saturations and pressures, and between phase relative permeabilities and saturations.

Multicomponent transport

We wish to consider transport of organic constituents which are subject to partitioning between water, oil, air and solid phases. Interphase transfer and transport of water and native soil gas constituents will be disregarded in the present analysis. To model component transport, continuity and mass flux equations for each partitionable component in each phase must be specified. Mass conservation of species α in the p-phase requires that:

$$\Phi(\partial c_{\alpha p} S_p / \partial t) = -\partial J_{\alpha p_i} / \partial x_i + R_{\alpha p} + \gamma_{\alpha p} \tag{5}$$

where $c_{\alpha p}$ is the concentration of the noninert component α in p-phase expressed as the mass of α per phase volume [$M L^{-3}$]; $J_{\alpha p_i}$ is the mass flux density of α in

p-phase per porous medium cross-section in the i-direction; $R_{\alpha p}$ is the net mass-transfer rate per porous medium volume of species α into (+) or out of (−) the p-phase [M L^{-3}]; and $\gamma_{\alpha p}$ is the net production (+) or decay (−) of α within phase p per porous medium volume due to reactions within the p-phase [M L^{-3}] described subsequently by:

$$\gamma_{\alpha p} = -\mu_{\alpha p} c_{\alpha p} \tag{6}$$

where $\mu_{\alpha p}$ is an apparent first-order rate coefficient.

The mass flux density of component α in phase p due to convection, diffusion and mechanical dispersion is described by:

$$J_{\alpha p_i} = c_{\alpha p} q_{p_i} - \Phi S_p D_{\alpha p_{ij}} \cdot \partial c_{\alpha p} / \partial x_j \tag{7}$$

where $D_{\alpha pij}$ is a dispersion tensor given by:

$$D_{\alpha p_{ij}} = g_{\alpha p}(D^{\text{dif}}_{\alpha p} + D^{\text{hyd}}_{p_{ij}}) \tag{8}$$

in which $D^{\text{dif}}_{\alpha p_{ij}}$ is the molecular diffusion coefficient of α in the porous medium; $D^{\text{hyd}}_{p_{ij}}$ is a mechanical dispersion coefficient; and $g_{\alpha p}$ is a nondilute solution correction factor. For the case of transport of low-solubility organic components, small volume fractions of organic components in water and aqueous phases will occur and $g_{\alpha w} = g_{\alpha a} = 1$ is assumed. For nonaqueous-phase liquids, the phase composition may reach 100% (e.g., single-component organic liquid) at which point dispersive transport becomes nonexistent. We accommodate nondilute solution diffusion–dispersion by approximating the oil-phase nonideal solution factor by:

$$g_{\alpha o} = 1 - c_{\alpha o}/\rho_o \tag{9}$$

Employing the tortuosity model of Millington (1959) and invoking the Stokes–Einstein equation to relate bulk diffusion coefficient to phase viscosity yields the expression for $D^{\text{dif}}_{\alpha p}$:

$$D^{\text{dif}}_{\alpha p} = \Phi^{1/3} S_p^{7/3} D^0_{\alpha w} / \eta_{rp} \tag{10}$$

where $D^0_{\alpha w}$ is the diffusion coefficient of α in bulk water; and η_{rp} is the ratio of p-phase viscosity to water-phase viscosity. The mechanical dispersion coefficient is assumed to be of the form (Bear, 1972):

$$D^{\text{hyd}}_{p_{ij}} = [\lambda_T \bar{q}_p \delta_{i,j} + (\lambda_L - \lambda_T)|q_{p_i} q_{p_j}|/\bar{q}_p]/\Phi S_p \tag{11}$$

where λ_L and λ_T are longitudinal and transverse dispersivity, respectively [L]; q_{p_i} and q_{p_j} are p-phase Darcy velocity in the i- and j-directions, respectively; $\bar{q}_p = |q_{p_i}|^{1/2}$ is the absolute magnitude of the p-phase velocity; and δ_{ij} is Kronecker's delta.

Combining the continuity and mass flux equations for transport of component α in the p-phase yields:

$$\Phi \frac{\partial c_{\alpha p} S_p}{\partial t} = \frac{\partial}{\partial x_i}\left[\Phi S_p D_{\alpha p_{ij}} \frac{\partial c_{\alpha p}}{\partial x_j}\right] - \frac{\partial c_{\alpha p} q_{\rho_i}}{\partial x_i} + R_{\alpha p} - \mu_{\alpha p} c_{\alpha p} \tag{12}$$

Expanding the first and third terms in eq. 12, employing the bulk p-phase continuity equation (1), and assuming density derivative terms to be of second-order importance yields:

$$\Phi S_p \frac{\partial c_{\alpha p}}{\partial t} = \frac{\partial}{\partial x_i}\left[\Phi S_p D_{\alpha p_{ij}} \frac{\partial c_{\alpha p}}{\partial x_j}\right] - q_{pi} \frac{\partial c_{\alpha p}}{\partial x_i} + R_{\alpha p} - (\mu_{\alpha p} + R_p/\rho_p) c_{\alpha p} \tag{13}$$

where the total phase mass-transfer rate, R_p, it may now be noted, is related to the individual component mass-transfer rates by:

$$R_p = \sum_{\alpha=1}^{n_s} R_{\alpha p} \tag{14}$$

where n_s denotes the number of "noninert" or partitionable species. For the three-fluid-phase system, eq. 13 constitutes a system of three equations which we may write for the water phase (p = w), the organic liquid phase (p = o) and the gas phase (p = a) as:

$$\Phi S_w \frac{\partial c_{\alpha w}}{\partial t} = \frac{\partial}{\partial x_i}\left[\Phi S_w D_{\alpha w_{ij}} \frac{\partial c_{\alpha w}}{\partial x_j}\right] - q_{w_i} \frac{\partial c_{\alpha w}}{\partial x_i} + R_{\alpha w} - (\mu_{\alpha w} + R_w/\rho_w) c_{\alpha w} \tag{15a}$$

$$\Phi S_o \frac{\partial c_{\alpha o}}{\partial t} = \frac{\partial}{\partial x_i}\left[\Phi S_o D_{\alpha o_{ij}} \frac{\partial c_{\alpha o}}{\partial x_j}\right] - q_{o_i} \frac{\partial c_{\alpha o}}{\partial x_i} + R_{\alpha o} - (\mu_{\alpha o} + R_o/\rho_o) c_{\alpha o} \tag{15b}$$

$$\Phi S_a \frac{\partial c_{\alpha a}}{\partial t} = \frac{\partial}{\partial x_i}\left[\Phi S_a D_{\alpha a_{ij}} \frac{\partial c_{\alpha a}}{\partial x_j}\right] - q_{a_i} \frac{\partial c_{\alpha a}}{\partial x_i} + R_{\alpha a} - (\mu_{\alpha a} + R_a/\rho_a) c_{\alpha a} \tag{15c}$$

To accommodate adsorption of α by the solid phase, an additional continuity equation is required which may be written as:

$$\partial c_{\alpha s}/\partial t = R_{\alpha s} - \mu_{\alpha s} c_{\alpha s} \tag{15d}$$

where $c_{\alpha s}$ is the solid-phase concentration expressed as mass of adsorbed component α per porous medium volume [$\mathrm{M\,L^{-3}}$]; $\mu_{\alpha s}$ is the first-order decay term ($\mathrm{T^{-1}}$) in the solid phase; and $R_{\alpha s}$ is the mass-transfer rate per porous medium volume to (+) or from (−) the solid phase [$\mathrm{M\,L^{-3}\,T^{-1}}$].

Phase-summed equation for local equilibrium transport

Coupling between the phase transport equations arises due to the interphase transfer terms. Explicit consideration of interphase transfer kinetics may often be justifiably avoided by assuming phase transfer to be equilibrium controlled. We consider here the case of linear partitioning and introduce the thermodynamic relations:

$$c_{\alpha o} = \Gamma_{\alpha o} c_{\alpha w} \tag{16a}$$

$$c_{\alpha a} = \Gamma_{\alpha a} c_{\alpha w} \tag{16b}$$

$$c_{\alpha s} = \Gamma_{\alpha s} c_{\alpha w} \tag{16c}$$

where $\Gamma_{\alpha o}$ is the equilibrium partition coefficient for species α between water and organic liquid (Raoult's constant); $\Gamma_{\alpha a}$ is the equilibrium partition coefficient between water and gas (dimensionless Henry's constant); and $\Gamma_{\alpha s}$ is a dimensionless equilibrium partition coefficient between water and solid phase.

Using the equilibrium relations, we may rewrite the phase transport equations in terms of a single-phase concentration. For water-wet systems, it is logical to retain the water-phase concentration since water will always be present in the system. Using eqs. 16 to eliminate oil-, gas- and solid-phase concentrations from eqs. 15 and summing the equations noting that:

$$R_{\alpha w} + R_{\alpha o} + R_{\alpha a} + R_{\alpha s} = 0 \tag{17}$$

leads to the phase-summed transport equation for species α:

$$L(c_{\alpha w}) \equiv \Phi^*_{\alpha} \frac{\partial c_{\alpha w}}{\partial t} - \frac{\partial}{\partial x_i}\left[D^*_{\alpha_{ij}} \frac{\partial c_{\alpha w}}{\partial x_j} \right] + q^*_{\alpha_i} \frac{\partial c_{\alpha w}}{\partial x_i} + \mu^*_{\alpha} c_{\alpha w} = 0 \tag{18a}$$

where

$$\Phi^*_{\alpha} = \Phi S_w + \Phi S_o \Gamma_{\alpha o} + \Phi S_a \Gamma_{\alpha a} + \Gamma_{\alpha s} \tag{18b}$$

$$D^*_{\alpha ij} = \Phi S_w D_{\alpha w_{ij}} + \Phi S_o D_{\alpha o_{ij}} \Gamma_{\alpha o} + \Phi S_a D_{\alpha a_{ij}} \Gamma_{\alpha a} \tag{18c}$$

$$q^*_{\alpha_i} = q_{\alpha w_i} + q_{\alpha o_i} \Gamma_{\alpha o} + q_{\alpha a_i} \Gamma_{\alpha a} \tag{18d}$$

$$\mu^*_{\alpha} = \mu_w + \mu_o \Gamma_{\alpha o} + \mu_a \Gamma_{\alpha a} + \mu_{\alpha s} \Gamma_{\alpha s} + R_w/\rho_w + R_o \Gamma_{\alpha o}/\rho_o + R_a \Gamma_{\alpha a}/\rho_a \tag{18e}$$

where $L(c_{\alpha w})$ is the differential operator describing phase-summed transport. Note that eqs. 18 have the same form as the classical single-phase transport equation. However, the coefficients represent pooled effects of transport in all phases. Note also that interphase masstransfer terms occur in the phase-summed equation only as a sum over all components.

Since we have assumed negligible gas-phase pressure gradients, only diffusive transport will be considered in the gas phase, i.e. $q_{ai} = 0$ will be assumed. It should be noted that even if gas pressure gradients have negligible effect on liquid phase flow, this does not strictly imply zero gas flow. If fluid saturations change in time, gas flow will occur. However, for the present analysis we constrain ourselves to situations for which gas convection effects should be of minor importance.

Initial and boundary conditions for transport equations

Initial and boundary conditions for the phase-summed transport equation need to be stipulated in terms of the water-phase concentration and are given as follows:

$$c_{\alpha w}(x_i, t = 0) = c_{\alpha w_0}(x_i), \quad \text{on } R \quad \text{for} \quad t = 0 \tag{19a}$$

$$c_{\alpha w}(x_i, t) = c_{\alpha w_1}(x_i, t), \quad \text{on } S_1 \quad \text{for} \quad t > 0 \tag{19b}$$

$$D^*_{\alpha_{ij}} \cdot \partial c_{\alpha w}/\partial x_j = 0, \quad \text{on } S_2 \quad \text{for} \quad t > 0 \quad (19c)$$

$$q_{wn} c_{\alpha w_3} + q_{on} c_{\alpha o_3} = q^*_n c_{\alpha w} - D^*_{\alpha_{ij}} \cdot \partial c_{\alpha w}/\partial x_j|_n, \quad \text{on } S_3 \quad \text{for} \quad t > 0 \quad (19d)$$

In eq. 19a $c_{\alpha w0}(x_i)$ represents the initial water-phase concentration of component α at location x_i. Eq. 19b describes a type-1 boundary condition on boundary segment S_1 with specified α-species water-phase concentration $c_{\alpha w_1}(x_i, t)$.

Note that stipulation of the water-phase concentration simultaneously fixes the organic liquid-, gaseous- and solid-phase concentrations under the assumption of local equilibrium. Eq. 19c describes type-2 boundaries with zero normal (n) concentration gradient specified on segment S_2. The zero gradient condition indicates zero normal dispersive flux at the boundary. If normal fluid velocities are nonzero, transport across the boundary will be permitted by convection. This boundary condition is commonly applied at boundaries which have fluid efflux to permit constituent transport across the boundaries. In the event that fluid fluxes are zero normal to the boundary, condition (19c) stipulates zero component flux. Eq. 19d is a type-3 boundary condition for use on boundary segments, S_3, which have inward fluid fluxes. Here, q_{on} and q_{wn} are the normal Darcy velocities of the oil phase and water phase, respectively, at the boundary and $c_{\alpha o_3}$ and $c_{\alpha w_3}$ are the concentrations of species α in the influent oil and water phase, respectively. In applying the type-3 boundary condition during periods of oil infiltration it is important to ensure consistency in the specified oil-phase concentrations such that:

$$\sum_{\alpha=1}^{n_s} c_{\alpha o} + c_{io} = \rho_o \quad (20)$$

where $c_{\alpha o}$ ($\alpha = 1, \ldots, n_s$) is the oil-phase concentration (expressed as mass component per phase volume) of partitionable component α; and c_{io} is the oil-phase concentration of "inert" (subscript i) or nonpartitionable components. Equivalently, in terms of mass fractions the condition to be met is:

$$f_{io} + \sum_{\alpha=1}^{n_s} f_{\alpha o} = 1 \quad (21)$$

where $f_{\alpha o}$ and f_{io} are the mass fraction of partitionable and inert components, respectively, in the oil-phase. Mass fractions and phase concentrations are related by:

$$c_{\alpha p} = f_{\alpha p} \rho_p \quad (22)$$

where ρ_p is the bulk phase density. Simple mixing theory permits component mass fractions and volume fractions to be related as:

$$c_{io}/\rho^0_o + \sum_{\alpha=1}^{n_s} c_{\alpha o}/\rho_\alpha = 1 \quad (23)$$

where ρ_α and ρ_o^0 are the density of pure noninert components and inert oil, respectively. The oil-phase density may accordingly be related to phase composition by:

$$\rho_o = \left(f_{io}/\rho_o^0 + \sum_{\alpha=1}^{n_s} f_{\alpha o}/\rho_\alpha \right)^{-1} \tag{24}$$

In applying the type-3 boundary condition, influent oil-phase concentrations, $c_{\alpha o3}$, must be specified such that eqs. 20–24 are obeyed.

In addition to the boundary conditions described by eqs. 19, externally controlled evaporative boundaries need to be handled as a type-3 condition with an atmospheric boundary layer (Sleep and Sykes, 1989). For such evaporative surfaces, the boundary condition can be written as:

$$(D_{\alpha a}^0/\chi)c_{\alpha a} = q_{\alpha n}^* c_{\alpha w} - D_{\alpha_{ij}}^* \cdot \partial c_{\alpha w}/\partial x_j|_n, \quad \text{on } S_4 \quad \text{for} \quad t > 0 \tag{25}$$

where $D_{\alpha a}^0$ is the boundary layer molecular diffusion coefficient taken to be equal to $D_{\alpha w}^0/\eta_{ra}$; and χ is the thickness of the atmospheric boundary layer. In the present work, we assume χ to be 1 cm.

Solution approach

Fluid flow equations are highly coupled with each other due to dependence of saturation and permeability of each phase on pressures in other phases necessitating a simultaneous solution approach. The flow equations are coupled with the transport equations via the occurrence of interphase mass-transfer terms and through dependence of fluid density and viscosity on fluid composition. Since mass-transfer rates are necessarily small for the case of low-solubility organic fluids and changes in fluid properties over short time periods will accordingly also be small, the dependence of the flow equations on transport will be very mild over short time spans permitting computational decoupling. Over extended periods of time, cumulative-phase mass transfer may have significant effects on flow as dissolution and volatilization deplete the nonaqueous phase liquid requiring some means of updating phase transfer rates and fluid properties. In the present analysis, we consider fluid compositional effects on phase density but regard phase viscosities to be constant.

The transport equations are highly dependent on the solution of the flow equations due to the occurrence of fluid velocity terms directly in the transport equations as well as indirectly due to the dependence of dispersion coefficients on fluid velocity and phase saturation. Thus, the flow equations must be solved concurrently with or prior to evaluating transport. Due to the weak back-coupling, the approach we take is to solve the transport equations serially with the flow equations. Furthermore, since the individual component transport equations are weakly coupled with each other in the present model due to the assumption of no reactions among components, transport equations may be solved serially in arbitrary sequence.

Our basic solution approach is as follows:

(1) Solve fluid flow equations simultaneously for current time step using time-lagged phase densities and interphase mass-transfer rates.

(2) Solve phase-summed transport equations serially for species 1, 2, ..., n_s using time-lagged phase densities and interphase mass-transfer rates for the same time step.

(3) Back-calculate interphase mass-transfer rates and update phase densities for current time step.

(4) Proceed to next time step.

The numerical model employed to solve the flow equations per step (1) above is as described by Kaluarachchi and Parker (1989) with addition of phase transfer terms as a source–sink function. Details of the flow solution will not be repeated here. In the following sections we describe the solution methodology for the phase-summed transport equations and for mass-transfer calculations and phase density updating.

Finite-element formulation

The phase-summed transport equations given by eqs. 18 are solved using an upstream weighted Galerkin finite-element method with linear rectangular elements. Assuming linear shape functions, N_I, the concentration $c_{\alpha w}$ can be approximated by:

$$c_{\alpha w}(x_i, t) = \sum_{J=1}^{4} N_J(\varepsilon, \eta) c_{\alpha w_J}(t) \tag{26}$$

where $c_{\alpha wJ}$ denotes the concentration at node J; and ε and η are local coordinates. Detailed information pertaining to the upstream weighting functions has been discussed by Kaluarachchi and Parker (1989). The Galerkin finite-element approximation of eqs. 18 over the entire domain R can be written as:

$$\int_R N_I L(c_{\alpha w})\, \mathrm{d}R = 0 \tag{27}$$

which leads to the set of equations given by:

$$[P]\{c_{\alpha w}\} + [M] \cdot \mathrm{d}c_{\alpha w}/\mathrm{d}t = \{R\} \tag{28}$$

Using the type-3 boundary condition given by eq. 19d and disregarding cross derivative terms, the matrices $[P]$, $[M]$ and $\{R\}$ are defined by:

$$P_{IJ} = \sum_{e=1}^{N} \int_{R_e} D^*_{\alpha_{ii}} \frac{\partial W_I}{\partial x_i} \frac{\partial N_J}{\partial x_i}\, \mathrm{d}R + \sum_{e=1}^{N} \int_{R_e} W_I q^*_{\alpha_i} \frac{\partial N_J}{\partial x_i}\, \mathrm{d}R + \sum_{e=1}^{N} \int_{R_e} N_I \mu^*_\alpha N_J\, \mathrm{d}R - \sum_{e=1}^{N_s} \langle q^*_n \rangle \int_{S_e} W_I N_J\, \mathrm{d}S \tag{29a}$$

$$M_{IJ} = \sum_{e=1}^{N} \int_{R_e} N_I \Phi^*_\alpha N_J\, \mathrm{d}R \tag{29b}$$

$$R_I = -\sum_{e=1}^{N_s} \langle q_{on} c_{\alpha o_3} + q_{wn} c_{\alpha w_3} \rangle \int_{S_e} W_I \, dS \tag{29c}$$

where N is the total number of elements; N_s is the total number of boundary elements; e refers to an element; W_I is the asymmetric upstream weighting function; and the term within angular brackets in eq. 29c is the average of $q_{on} c_{\alpha o3} + q_{wn} c_{\alpha w3}$ over the side of the element where contaminant enters the system on surface S_3. If an evaporative boundary is present, the term $\langle q^*_n \rangle$ in eq. 29a will have an additional term of $(-D^0_{\alpha a} \Gamma_{\alpha a})$ to account for the atmospheric boundary layer and the terms within $\langle\ \rangle$ in eq. 29c will vanish. Treatment of the integrals in eq. 28 employs the method of influence coefficients described by Kaluarachchi and Parker (1989) which will not be repeated here.

Phase-summed velocities in a three-fluid-phase system can be highly non-uniform due to the complex nature of multiphase fluid flow. Conventional element integration methods may not provide accurate results under such conditions with respect to nodal concentrations and mass balance due to numerical oscillations. To dampen any numerical problems associated with the convective term, we represent the velocity within an element by:

$$q^*_{\alpha_i}(x_i, t) = \sum_{L=1}^{4} N_L(\varepsilon, \eta)\, q^*_{\alpha_{iL}}(t) \tag{30}$$

where $q^*_{\alpha_{iL}}$ is the phase-summed velocity at Gauss point L. Using eqs. 29 on the convective term of eq. 28a and using linear upstream weighting shape functions (Kaluarachchi and Parker, 1989), it is possible to show that:

$$\sum_{e=1}^{N} \int_{R_e} W_I q^*_{\alpha_i} \frac{\partial N_J}{\partial x_i} \, dR = \sum_{e=1}^{N} \sum_{L=1}^{4} \left[\tfrac{1}{2} m \{[H^{xg}]_L + [H^{xu}]_L\} + \tfrac{1}{2} d \{[H^{yg}]_L + [H^{yu}]_L\}\right] \tag{31}$$

where m and d are the width and height of a rectangular element, respectively; x and y are the coordinate axes; and matrices $[H]$ with superscripts xg and yg refer to the contributions from standard linear shape functions, while matrices with superscripts xu and yu refer to contributions from upstream weighting coefficients. Details of matrices $[H]$ are given in the Appendix.

The surface integrals in eqs. 29a and 29c can be described by:

$$\int_{S_e} W_I N_J \, dS = \tfrac{1}{12} l (4 \pm 3\omega) \quad \text{if} \quad I = J \tag{32a}$$

$$= \tfrac{1}{12} l (2 \pm 3\omega) \quad \text{if} \quad I \neq J \tag{32b}$$

and

$$\int_{S_e} W_I \, dS = \tfrac{1}{2} l (1 \pm \omega) \tag{32c}$$

where l is the length of the side; and ω is the upstream weighting coefficient. The appropriate sign of the integrals given in eqs. 32 will be determined by the side of the element exposed to the boundary condition.

Time integration of eq. 28 is performed using a standard finite-difference approximation. The resulting final set of equations can be written as:

$$\{\theta[P] + [M]/\Delta t_{K+1}\}^{K+\theta} \{c_{\alpha w}\}^{K+1} = \{[M]/\Delta t_{K+1} + (\theta - 1)[P]\}^{K+\theta} \times \{c_{\alpha w}\}^{K} + \{R\}^{K+\theta} \quad (33)$$

where K and $(K + 1)$ refer to previous and current time steps, respectively; and θ is a time weighting factor. In the present work, we use a Crank–Nicolson time stepping scheme corresponding to $\theta = 0.5$ to provide an unconditionally stable second-order accurate temporal approximation. Time step size is varied under program control by a time incremental factor which increases or decreases time step size depending on the number of iterations required for solution of the flow problem. The size of the time steps employed for solution of the transport equation may vary as an integral factor of that used for the flow problem. In the present paper, the transport time step is taken to be half of the time step used for the flow problem to reduce numerical oscillation and dispersion in the transport solution by lowering the effective element Courant and Péclet numbers. With this procedure, linearly interpolated velocities and other parameters between K and $(K + 1)$ flow solution time levels were used to perform the simulation at intermediate time levels for the transport solution. The governing equations describing the simultaneous flow and transport in two-dimensional radial symmetric domains in r–z coordinates are similar to eqs. 3 and 18 and will not be repeated here. The finite-element analysis is performed in an identical manner to that described previously by using the average radial distance to a given node or Gauss point within an element (Huyakorn and Pinder, 1983) to avoid costly numerical integration.

Computation of interphase mass-transfer rates

Mass transfer between phases plays an important role in modeling multiphase transport since it controls the liquid-phase distribution of contaminant which serves as a long-term source of contamination within the porous medium. Mass-transfer rate terms are the principal mode of coupling between flow and transport equations. Specifically, the terms which are required to solve eqs. 4 and 18 are the component-summed mass-transfer rates for water, oil and air phases: R_w, R_o and R_a, respectively.

Since these terms are time-lagged, updating is performed at the end of a time step after solving the flow and transport equations using previous time step mass-transfer rates. Updating of the mass-transfer rates is accomplished by back-substituting component concentrations obtained from the solution of the phase-summed transport equation (18) and the equilibrium relations (16) into the individual phase transport equations (12) to compute new component

mass-transfer rates $R_{\alpha w}$, $R_{\alpha o}$ and $R_{\alpha a}$ which may then be summed over all components via eq. 14 to obtain updated R_w, R_o and R_a.

Decoupling of flow and transport equations in this fashion has the advantage of computational efficiency. The disadvantage is that if appreciable errors occur in computed mass-transfer terms they will propagate to the flow solution, which may in severe cases result in numerical instability. Since back-calculation of mass-transfer rates requires numerical evaluation of spatial derivatives of Darcy velocities and dispersive fluxes (see eq. 12), difficulties can arise during periods of highly transient flow conditions when sharp velocity and concentration fronts arise. This is particularly true during oil infiltration periods since small errors in water concentration and/or oil phase Darcy velocity will be magnified during back-substitution by the partition coefficient $\Gamma_{\alpha o}$ which is typically on the order of $\geqslant 10^3$. To circumvent these difficulties, we make two modifications in the scheme for computing mass-transfer rates.

(1) During periods of high oil flow, mass-transfer rates are set to zero and no updating is performed. Operationally, the criterion that is tested is whether resultant oil velocity at all nodes is less than a fraction, f_{crit}, of:

$$K_{so} = (K_{sw_x} + K_{sw_y})/2\eta_{ro}$$

For problems involving spills which occur over short periods of time followed by redistribution under natural hydraulic conditions, oil flow rates rapidly diminish as a "residual saturation" state is approached. Since total mass transfer over short time spans will be necessarily small, disregarding mass-transfer terms during highly transient flow periods will have minor effects on the coupled problem solution. For simulations in this paper, a value of $f_{crit} = 0.0001$ was used.

(2) When mass-transfer terms are computed, a global mass-balance check is performed for each component by comparing directly computed boundary fluxes with changes in mass over a time step determined from spatial integration of nodal concentrations and saturations. Mass-transfer rates computed by back-substitution in eq. 12 are then corrected in proportion to the global mass-balance error. This correction ensures that mass-transfer terms time-lagged in the flow equation meet a global mass-balance constraint.

Compositional dependence of fluid properties

Updating of phase densities. With increasing simulation time, the density of each phase will change depending on the net mass of each component leaving or entering the phase. Although density derivatives were neglected in the equation development on the assumption that these terms are small over a given time step, cumulative changes in density cannot be ignored since over long times these can accumulate and become quite large. To accommodate these effects, phase densities are updated at the end of each time step as follows:

$$\rho_w = \rho_w^0 \left(1 - \sum_{\chi=1}^{n_s} c_{\chi w}/\rho_\chi\right) + \sum_{\chi=1}^{n_s} c_{\chi w} \tag{34a}$$

$$\rho_o = \rho_o^0 \left(1 - \sum_{\chi=1}^{n_s} c_{\chi o}/\rho_\chi\right) + \sum_{\chi=1}^{n_s} c_{\chi o} \tag{34b}$$

$$\rho_a = \frac{P_{atm}\,\rho_a^0}{RT}\left(\frac{\rho_a^0 + \sum_{\chi=1}^{n_s} c_{\chi a}}{\rho_a^0/M_a^0 + \sum_{\chi=1}^{n_s} c_{\chi a}/M_\chi}\right) \tag{34c}$$

where n_s again denotes the number of "noninert" or partitionable species; ρ_w^0 is the density of uncontaminated water; ρ_χ is the density of pure χ-component; ρ_o^0 is the density of "inert" oil components; P_{atm} is atmospheric pressure; R is the universal gas constant; T is Kelvin temperature; M_a^0 and ρ_a^0 are the molecular weight and density of pure air, respectively; and M_χ is the molecular weight of component χ. Density ratios, ρ_{rw} and ρ_{ro}, are computed as the ratio of ρ_w or ρ_o to ρ_w^0.

Viscosity and scaling parameters. Fluid viscosities and surface tension ratios required to describe saturation–capillary pressure function relations (Lenhard and Parker, 1987) are assumed to be constants for a simulation. For a given simulation, these parameters are computed based on the initial fluid composition and are not updated. The air–oil and oil–water scaling factors (i.e. surface tension ratios), β_{ao} and β_{ow}, and the viscosity ratio, η_{ro}, are calculated as:

$$\beta_{ao} = \sigma_w \Big/ \left(f_{io}\sigma_o^i + \sum_{\chi=1}^{n_s} f_{\chi o}\sigma_o^\chi\right) \tag{35a}$$

$$\beta_{ow} = 1/(1 - \beta_{ao}^{-1}) \tag{35b}$$

$$\eta_{ro} = f_{io}\eta_{ro}^i + \sum_{\chi=1}^{n_s} f_{ao}\eta_{ro}^\chi \tag{35c}$$

where σ_w is the surface tension of pure water; σ_o^i and σ_o^χ are surface tension of the inert fraction and each noninert component χ, respectively; and η_{ro}^i and η_{ro}^χ are the viscosity ratio of the inert fraction and each noninert component χ, respectively. Eq. 35b was obtained from the multiphase constitutive relationships described by Parker et al. (1987) assuming negligible differences between contaminated and uncontaminated water surface tensions. Assuming the parameters β_{ao}, β_{ow} and η_{ro} to be time invariant during a simulation is not strictly correct. However, since organic flow generally occurs over a relatively short period of time following a spill event and before reaching residual saturation, effects of compositional changes on flow analysis will not generally be of great importance.

TABLE 1

Soil hydraulic and bulk fluid properties* of example problems

Parameter	Example I	Example II	Example III
Φ	0.4	0.4	0.4
n	2.5	2.0	2.0
S_m	0	0	0
α (L^{-1})	0.05	0.8	0.8
K_{sw_x} (LT^{-1})	–	3.0	2.0
K_{sw_y} (LT^{-1})	40.0	3.0	2.0
ρ_{ro}	0.8	0.85	1.47
η_{ro}	2.0	2.0	0.58
β_{ao}	2.69	2.61	2.34
β_{ow}	1.59	1.62	3.02
ε_L (L)	0.4	0.4	0.2
ε_T (L)	0.05	0.06	0.02

* Units for example I are cm and h; examples II and III in m and days.

HYPOTHETICAL NUMERICAL SIMULATIONS

The multiphase flow code MOFAT-2D described by Kaluarachchi and Parker (1989) was extended to accommodate the proposed transport model and was verified against simple single-phase transport problems using analytical solutions. To demonstrate the applicability and effectiveness of the proposed model, a number of one- and two-dimensional simulations involving single- and multicomponent transport were performed which will be described in this section. Soil and fluid properties used in the simulations are given in Table 1. Three-phase flow relations are described by the model of Parker et al. (1987) in which α, n and S_m are parameters of the air–water saturation–capillary pressure function and β_{ao} and β_{ow} are fluid-dependent scaling factors. Oil-phase scaling factors and viscosities were computed as mass fraction weighted averages of component values corresponding to the initial oil composition for

TABLE 2

Properties of organic components in example problems

Parameter	Benzene	Toluene	Chloropropane	TCE	"Inert"
D^0_{zw} (cm^2h^{-1})	0.04	0.04	0.04	0.04	–
Γ_{zo}	494	1,674	330	1,336	–
Γ_{za}	0.17	0.26	0.54	0.38	–
Γ_{zs}	0	0	0	0	–
ρ_z ($mg\,cm^{-3}$)	877	862	891	1,470	800
M_z ($mg\,mol^{-1}$)	780	920	790	1,310	–
η^z_{ro}	2.0	2.0	2.0	0.58	2.0
σ^z_o ($dyn\,cm^{-2}$)	29	28.5	30	30.7	25

each example and were assumed to remain constant during the simulation period (see eqs. 35). Properties of organic-phase constituents employed in the simulations are given in Table 2. Phase densities, Henry's constants and water-phase diffusion coefficients were obtained from the literature for the various compounds. Raoult's constant, $\Gamma_{\chi o}$, was estimated as the ratio of pure liquid-phase density, ρ_χ, to water solubility, $c_{\chi w}^{max}$.

Example I: One-dimensional two-component transport without volatilization

A 75-cm-long vertical column of sandy soil is considered in this problem involving an initially oil-free system in equilibrium with a water table located 50 cm from the top surface. A slug of organic liquid containing 28% mass fraction of benzene, 19% toluene and 53% inert components was introduced at the upper surface under a water-equivalent head of 1 cm until a total oil accumulation of 1.5 $cm^3 cm^{-2}$ was achieved. The lower boundary was maintained at the initial head for the water-phase and the oil-phase was specified as zero flux. Boundary conditions for the transport problem were zero dispersive flux at the bottom boundary at all times and a type-3 condition at the upper surface. From the data in Table 2 and eq. 24, the density of oil entering the system is 832 mg cm^{-3} and from eq. 22 $c_{\chi o_3}$ for influent oil is 247 mg cm^{-3} for benzene and 167 mg cm^{-3} for toluene.

Following the oil infiltration period, a water flux of 0.12 cm h^{-1} was introduced at the upper surface and a zero-flux condition was maintained for the oil phase. Assuming uncontaminated water enters the system and no evaporation occurs, a type-3 condition was imposed at the upper surface during water infiltration with $c_{\chi w_3} = 0$ resulting in zero total component flux across the boundary. Note that use of a type-2 condition for the phase-summed equation during water infiltration would result in an apparent component flux into the system equal to the product of water flux density and surface concentration in the water phase. Lower boundary conditions after the oil infiltration event remained as previously described.

A finite-element mesh of 55 elements was used in the simulations. The initial time step used in the simulations was 0.001 h which was allowed to increase to a maximum time step of 1.0 h. Upstream weights of 0.2 were used in the simulations. To demonstrate the effects of mass transfer between phases, the simulation was performed with and without updating for mass transfer and phase density. For both simulations, the time required for 1.5 cm of oil to enter the system was 0.051 h, at which instant the total masses of benzene and toluene in the system computed from space integration of concentration distributions were 374 and 254 mg, respectively, corresponding to mass-balance errors of $\sim 0.3\%$.

Fig. 1 shows component masses apparently lost from the system after the end of the oil infiltration period due to outflow from the lower boundary computed from space integrals of component concentrations. Also shown are global mass-balance errors computed as the differences between mass losses

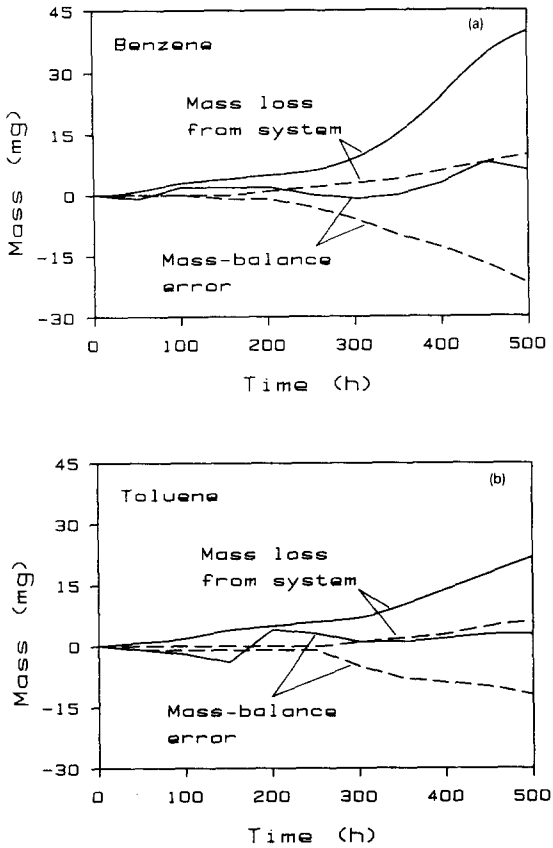

Fig. 1. Total mass lost from the column computed from spatial integration of concentrations and global mass-balance error with and without updating for mass transfer for example I: (a) benzene and (b) toluene.

calculated from concentration space integrals and those obtained directly from computed boundary fluxes. For each component it is seen that mass loss via concentration space integrals is under-predicted when mass-transfer updating is disregarded, thereby resulting in a continuously increasing global mass-balance error. For simulations with mass-transfer updating, the global mass-balance error remained small and fluctuated with time over the 500-h simulation period.

Distributions of water-phase benzene and toluene concentrations at the end of the 500-h simulation with mass-transfer updating are shown in Fig. 2. Except for some numerical undershoot at the lower boundary, water-phase concentrations are constant at the initial concentrations of 0.5 and 0.1 mg cm^{-3} for benzene and toluene, respectively, over the lower region of the column. Toluene extraction from the porous medium has occurred to an average depth of ~ 10 cm, whereas the "extraction front" for benzene extends to ~ 20 cm, reflecting the greater solubility for the latter species. Water and total liquid

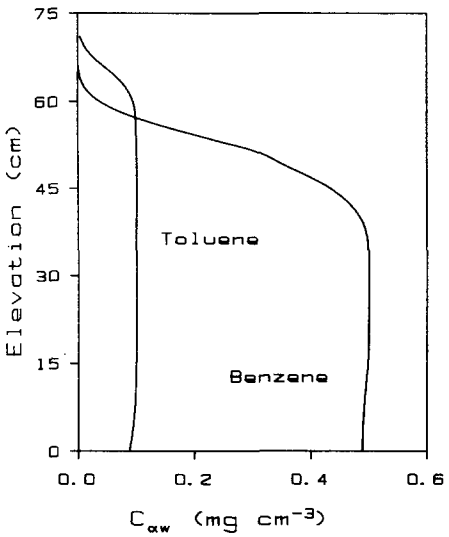

Fig. 2. Distribution of water-phase benzene and toluene concentrations at 500 h for example I with mass-transfer updating.

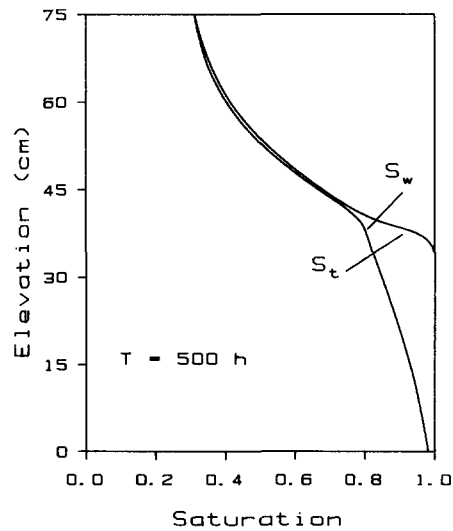

Fig. 3. Distribution of liquid saturations at 500 h for example I; S_t and S_w refer to total liquid and water saturations, respectively.

saturation distributions at 500 h for the simulation with mass-transfer updating are shown in Fig. 3. Due to the influx of water from the upper surface, oil saturation remained almost zero in the vicinity of the upper surface and most of the oil has been displaced towards the lower surface. Also due to the continuous application of the water at the upper surface, the zero water pressure elevation ("oil–water table") has risen from its initial depth of 50 cm

to ~40 cm. The simulation with mass-transfer updating predicted a total oil-phase loss due to dissolution and convective fluxes at the lower surface equal to 0.1 $cm^3 cm^{-2}$ which corresponds to 6.7% of the infiltrated volume. Final mass losses of individual components relative to their respective infiltrated masses computed from the simulation with mass-transfer updating were 10.7% for benzene and 8.7% for toluene.

Example II: Two-dimensional two-component transport under natural hydraulic conditions with covered surface

In this example, we demonstrate the effects of fluid properties on aqueous and gaseous plume migration following a spill of low-density hydrocarbon into a silty soil. The domain is a 25 m × 12 m vertical slice through the unsaturated and saturated zones (Fig. 4). The initial condition corresponds to an air–water system with a sloping water table and vertical equilibrium pressure distributions. The simulation involves infiltration of ~5 $m^3 m^{-1}$ of oil containing 28% mass fraction of benzene, 28% chloropropane and 44% inert oil followed by redistribution under natural hydraulic conditions for 30 days. The soil properties and transport parameters used in the simulation are given in Tables 1 and 2. For the flow analysis, a zero flux condition was assumed along *AH, BC, GF, CD* and *EF* for both phases. On segment *DE*, oil was allowed to infiltrate under a water-equivalent head of 1 cm and thereafter was maintained at zero flux. For the water-phase, *DE* remained at zero flux at all times. On segments *AB* and *HG*, a type-1 condition was assumed for the water phase corresponding to the initial pressure heads and a zero-flux condition was imposed for the oil phase. Boundary conditions for the transport analysis consist of a type-3 condition along *DE* with influent oil-phase concentrations of benzene and chloropropane equal to 247 mg cm^{-3} during oil infiltration and zero during redistribution. On the remaining boundaries, a zero-dispersive flux condition was assumed during the entire simulation. Note that the surface boundary condition simulates a covered surface which does not permit water infiltration, water evaporation or organic component evaporation. A finite-element mesh consisting of 513 elements and an upstream weighting factor of 0.15 was used

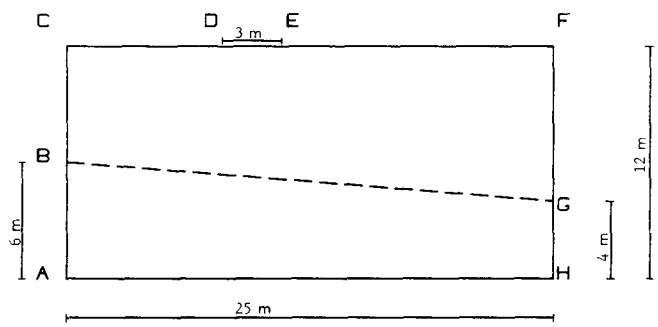

Fig. 4. Two-dimensional flow domain used in example II.

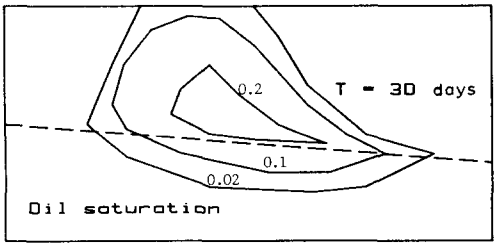

Fig. 5. Distribution of oil saturations at 30 days in example II.

in the simulation. The initial time step for the simulation was 0.001 day which was allowed to increase to a maximum time step of 0.25 day with an incremental factor of 1.03.

The results indicated that the prescribed oil volume of $5\,m^3\,m^{-1}$ entered the system in 1.37 days at which time the total mass of benzene and chloropropane in the system was 1238 kg. Predicted oil saturations after 30 days of redistribution are shown in Fig. 5. At this time oil-phase movement has virtually ceased due to the low relative permeability associated with diminishing fluid saturation. Due to the high viscosity and low density ratios of the oil mixture, the oil phase penetrates very little below the original air–water table as it spreads laterally along the natural hydraulic gradient. The highest oil saturation at the end of 30 days was ~ 0.2 and this occurred in a region located under the original spill site. Predicted water-phase concentrations of benzene and chloropropane at 30 days are shown in Fig. 6. The patterns of the aqueous-phase concentrations are similar for both components, but at a given location the concentration of chloropropane is ~ 1.5 times greater than that of benzene.

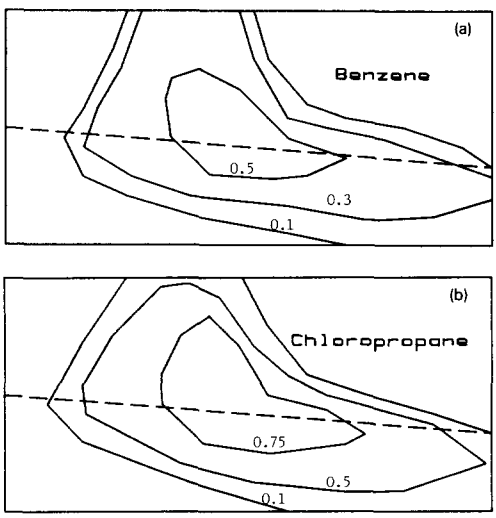

Fig. 6. Distribution of water-phase concentrations (mg cm^{-3}) at 30 days for example II: (a) benzene and (b) chloropropane.

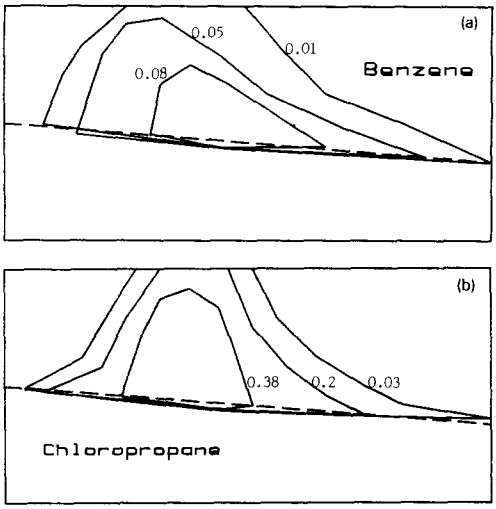

Fig. 7. Distribution of gas-phase concentrations (mg cm^{-3}) at 30 days for example II: (a) benzene and (b) chloropropane.

The higher concentration of chloropropane reflects the higher Raoult's constant, $\Gamma_{\alpha o}$, of benzene. The results show that, although the oil-phase plume itself does not move far from the spill site, dissolution and volatilization results in growing aqueous- and gaseous-phase plumes migrating in the direction of groundwater flow.

Predicted gas-phase concentrations of the two components at 30 days show a similarity in overall distributions as was the case for the aqueous phase. Gas-phase concentrations of chloropropane exceed those of benzene roughly in proportion to the air–oil partition ratio $\Gamma_{\alpha a}/\Gamma_{\alpha o}$ for the two components (Fig. 7).

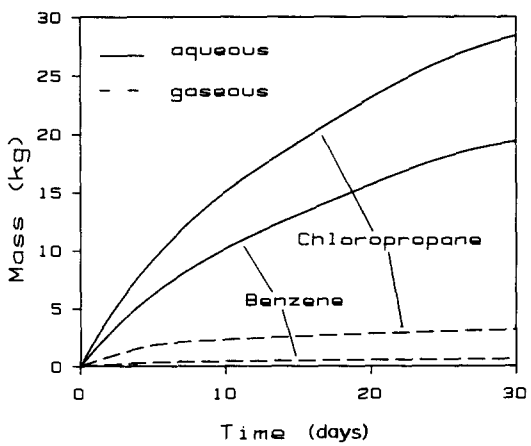

Fig. 8. Cumulative mass of contaminant removed from system via the aqueous and gaseous phases in example II.

Cumulative masses of benzene and chloropropane dissolved in the water phase and volatilized into the gas phase over the 30-day period are shown in Fig. 8. Due to the higher solubility and air–oil partition ratio of chloropropane, its rate of aqueous- and gaseous-phase mass transfer is always higher than for benzene. At the end of the simulation, the rates of aqueous-phase partitioning appear to be approaching steady-state values of ~ 0.3 kg day^{-1} for chloropropane and 0.2 kg day^{-1} for benzene. Final global rates of gas-phase mass transfer are ~ 0.035 and ~ 0.009 kg day^{-1} for chloropropane and benzene, respectively. At the end of the 30-day period, the total mass of benzene lost from the oil phase was $\sim 1.4\%$ of the original benzene mass while the corresponding value for chloropropane was $\sim 2.5\%$. Extrapolation of the final mass-transfer rates indicates that benzene and chloropropane release from the oil plume will continue for 10–15 yr. Since mass-transfer rates will actually continue to decrease as oil-phase concentrations diminish (see Fig. 8), the actual release duration will be longer.

Example III: Two-dimensional transport of dense NAPL with water pumping and volatilization

In the present example, we consider a spill of pure trichloroethylene (TCE) in a homogeneous silty soil. Following infiltration and redistribution of the organic phase under natural hydraulic conditions, remediation is pursued by water pumping abetted by volatilization at the soil surface through a diffusion boundary layer. The flow domain involves a 15-m-tall radial section with an inner radius of 0.1 m and an outer radius of 12.1 m (Fig. 9). Initial conditions correspond to an air–water system in hydrostatic equilibrium with a horizontal

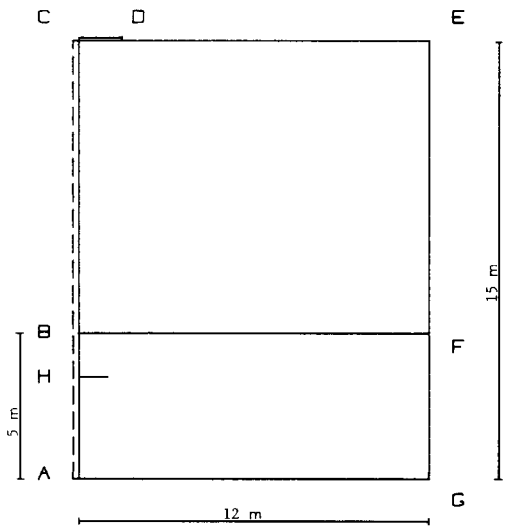

Fig. 9. Two-dimensional flow domain used in example III. *Dotted line* shows center line of 20-cm-diameter well.

water table (BF) located 5 m above the lower surface. Simulation of flow and transport of TCE for this problem was performed in three stages:

(1) Infiltration of TCE along segment *CD* under a water-equivalent oil head of 1 cm until the total accumulation was $\sim 5.9\,m^3$.

(2) Redistribution of TCE for 21 days with zero flux conditions for water and oil phases on boundaries. Volatilization of contaminant from the upper surface was allowed via a boundary diffusion layer of 1-cm thickness.

(3) Initiate water pumping on the inner radius such that the water level in the well is maintained 1.5 m below the initial water level (BF) for a 100-day period together with volatilization from the upper surface.

Additional boundary conditions for the flow problem are zero flux for the water phase along the segments *BC, CE, EF* and *AG* and constant water heads equal to the initial values on *GF* at all times. For the oil phase, a zero-flux condition was assumed along the entire boundary at all times except during infiltration on *CD*. Type-3 transport boundary conditions were stipulated on segment *CD* with $c_{\alpha o_3} = 1470\,mg\,cm^{-3}$ during oil infiltration corresponding to pure TCE. On segment *FG* a type-3 condition with $c_{\alpha w_3} = 0$ was imposed corresponding to inflow of uncontaminated water on the outer perimeter. Volatilization via a surface boundary layer was allowed on *CE* during stages 2 and 3. Zero dispersive flux was imposed on all other boundaries. Soil hydraulic and transport properties used in the simulation are given in Tables 1 and 2. The simulation was performed with a finite-element mesh of 420 elements and time step size varying between 0.001 and 0.5 day during the simulation period.

The results of the simulation showed that 5.9 m of TCE infiltrated the soil in 1.13 days. Predicted oil saturation contours at 21 and 121 days are shown in Fig. 10. Results at 21 days indicate maximum oil saturations of ~ 0.16. High saturations occur above the capillary fringe, decrease to low values in the upper saturated zone and again increase at the lower aquifer boundary where lateral spreading occurs. Drainage of TCE from the unsaturated zone

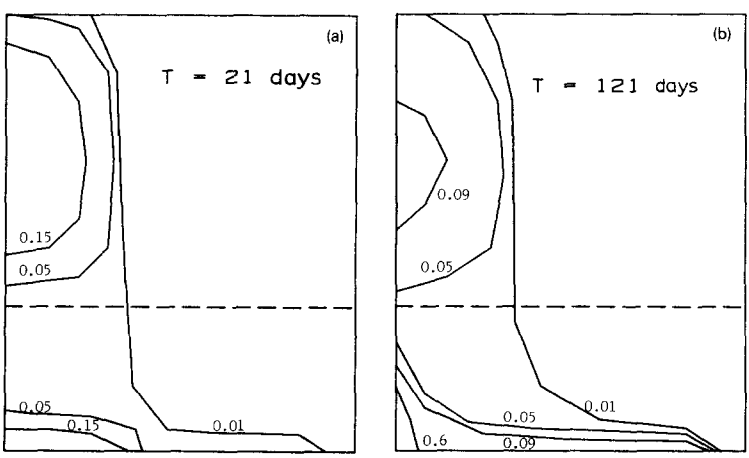

Fig. 10. Distribution of oil saturations in example III: (a) at 21 days and (b) 121 days.

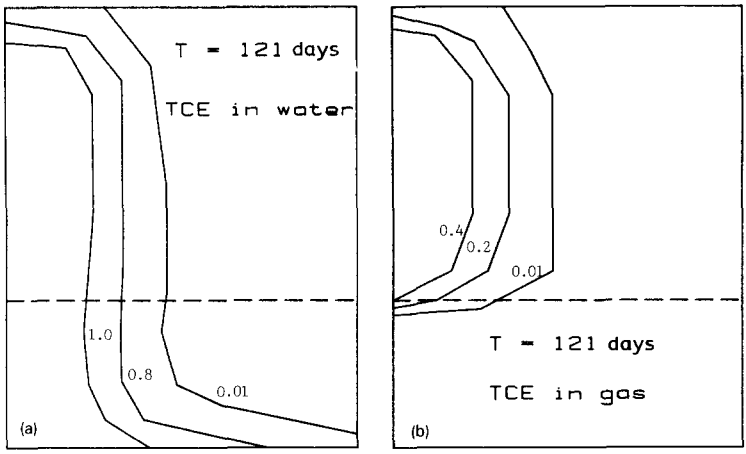

Fig. 11. Distribution of TCE concentrations (mg cm^{-3}) at 121 days for example III in: (a) water phase and (b) gas phase.

continued after 21 days and water pumpage produced a build-up of liquid TCE near the well bore at the aquifer lower boundary. The predicted water-phase concentration distribution of TCE at 121 days (Fig. 11a) indicates lowered water-phase concentration towards the right-hand boundary due to the water moving into the domain from the right-hand boundary under the imposed hydraulic gradient. Due to the mild impedance caused by the atmospheric boundary layer, a fairly sharp gas-phase concentration gradient occurs near the soil surface (Fig. 11b). Radial spreading of TCE in the gas phase occurs little beyond the liquid-phase plume.

Cumulative masses of TCE removed from the soil–aquifer system vs. time via the water phase (i.e. water pumpage at the well bore) and via the gas phase (i.e. volatilization at the soil surface) are shown in Fig. 12. During the first 21 days,

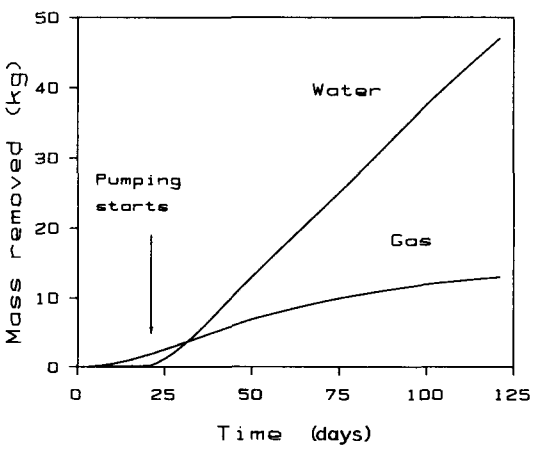

Fig. 12. Mass of TCE removed from system via water and gas phases in example III.

a small amount of TCE was removed by volatilization with the vapor loss rate reaching a maximum of 0.18 kg day^{-1} between 20 and 50 days and then gradually decreasing to $\sim$0.06 kg day^{-1} by the end of the simulation. The steady-state water pumping rate under the imposed well bore pressure predicted removal of TCE via the water phase at a nearly constant rate of 0.47 m^3 day^{-1}. The rate is constant due to the saturated water-phase concentration of TCE at the well bore equal to the solubility and almost constant water velocities along the well bore during the 100-h period. Over the 121-day simulation period, 0.6% of the total TCE mass was removed by water pumping and 0.12% by surface volatilization. Extrapolation of the final mass removal rates indicates that complete removal of TCE would be accomplished after $\sim$50 yr. However, if pumping was continued over a long period of time, the water-phase concentration at the well bore would eventually fall below the solubility limit, thereby decreasing the TCE removal rate.

CONCLUSIONS

A previously developed two-dimensional finite-element model to predict flow of water and organic liquid in three-fluid-phase porous media was extended to simulate transport of multicomponent organic contaminants, assuming local equilibrium phase partitioning. The latter assumption reduces the computational effort significantly by reducing the individual phase transport equations to a single phase-summed equation per component. Mild coupling between the flow and the transport equations enables a decoupled solution approach by using time-lagged phase densities and interphase mass-transfer rates. Interphase mass-transfer rates are computed by direct substitution of the computed concentrations in the individual phase transport equations and corrected for global mass-balance errors. Updating for time-lagged interphase mass-transfer rates is considered only after the oil-phase velocities reach a pre-defined critical value to avoid numerical instabilities caused by imprecision in computed mass-transfer rate when oil velocity is high. Simulation results indicate that interphase mass-transfer rate computations and density updating will not have significant effects on mass partitioning during short-term transient flow conditions (e.g. during a spill event). However, over the long term, mass transfer between phases has significant cumulative effects and needs to be taken into account to maintain a global mass balance. The transport properties of individual noninert components of an organic mixture play an important role in predicting the overall distribution of the contaminants in different phases.

Simulation results indicate that contaminant losses due to volatilization from the soil surface will not significantly reduce the total mass of contaminant in the subsurface unless the spill is very small. Removal by water pumping is more effective, but may still take many years to achieve cleanup due to the low solubility of common organic contaminants. Improved efficiency may be feasible by employing combined water- and gas-phase pumping. In future

studies, we will investigate model extensions to consider effects of gas-phase dynamics on multiphase organic chemical transport.

ACKNOWLEDGEMENTS

This work was sponsored by the U.S. EPA R.S. Kerr Environmental Research Laboratory under cooperative agreement CR-812073-01.

APPENDIX

$$[H^{xg}]_1 = \frac{1}{36}\begin{bmatrix} -6 & 6 & 2 & -2 \\ -3 & 3 & 1 & -1 \\ -1 & 1 & 1 & -1 \\ -2 & 2 & 2 & -2 \end{bmatrix} \qquad [H^{xg}]_2 = \frac{1}{36}\begin{bmatrix} -3 & 3 & 1 & -1 \\ -6 & 6 & 2 & -2 \\ -2 & 2 & 2 & -2 \\ -1 & 1 & 1 & -1 \end{bmatrix}$$

$$[H^{xg}]_3 = \frac{1}{36}\begin{bmatrix} -1 & 1 & 1 & -1 \\ -2 & 2 & 2 & -2 \\ -2 & 2 & 6 & -6 \\ -1 & 1 & 3 & -3 \end{bmatrix} \qquad [H^{xg}]_4 = \frac{1}{36}\begin{bmatrix} -2 & 2 & 2 & -2 \\ -1 & 1 & 1 & -1 \\ -1 & 1 & 3 & -3 \\ -2 & 2 & 6 & -6 \end{bmatrix}$$

$$[H^{xu}]_1 = \frac{\alpha}{24}\begin{bmatrix} 3 & -3 & -1 & 1 \\ -3 & 3 & 1 & -1 \\ -1 & 1 & 1 & -1 \\ 1 & -1 & -1 & 1 \end{bmatrix} \qquad [H^{xu}]_3 = \frac{\alpha}{24}\begin{bmatrix} 1 & -1 & -1 & 1 \\ -1 & 1 & 1 & -1 \\ -1 & 1 & 3 & -3 \\ 1 & -1 & -3 & 3 \end{bmatrix}$$

$$[H^{xu}]_2 = [H^{xu}]_1 \qquad [H^{xu}]_4 = [H^{xu}]_3$$

REFERENCES

Abriola, L.M., 1984. Multiphase migration of organic compounds in a porous medium – A mathematical model. C.A. Brebbia and D.A. Orszag (Editors), Lecture Notes in Engineering, Vol. 8. Springer, New York, NY, p. 232.

Abriola, L.M. and Pinder, G.F., 1985. A multiphase approach to the modeling of porous media contamination by organic compounds, 1. Equation development. Water Resour. Res., 21: 11–18.

Bear, J., 1972. Dynamics of Fluids in Porous Media. American Elsevier, New York, NY, 764 pp.

Corapcioglu, M.Y. and Baehr, A.L., 1987. A composition multiphase model for groundwater contamination by petroleum products, 1. Theoretical considerations. Water Resour. Res., 23: 191–200.

Falta, R.W. and Javandel, I., 1987. A numerical method for multiphase multicomponent contaminant transport in groundwater systems. Eos (Trans. Am. Geophys. Union), 68(44): 1284 (abstract).

Faust, C.R., 1985. Transport of immiscible fluids within and below the unsaturated zone: Numerical model. Water Resour. Res., 21: 587–596.

Hochmuth, D.P. and Sunada, D.K., 1985. Groundwater model of two phase immiscible flow in coarse material. Ground Water, 23: 617–626.

Huyakorn, P.S. and Pinder, G.F., 1983. Computational Methods in Subsurface Flow. Academic Press, San Diego, CA, 473 pp.

Jury, W.A., Spencer, W.F. and Farmer, W.J., 1983. Behavior assessment model for trace organics in soil, I. Model description. J. Environ. Qual., 12(4): 558–564.

Kaluarachchi, J.J. and Parker, J.C., 1989. An efficient finite element method for modeling multiphase flow. Water Resour. Res., 25: 43–54.

Kaluarachchi, J.J., Parker, J.C. and Lenhard, R.J., 1990. A numerical model for water and light hydrocarbon migration in unconfined aquifers under vertical equilibrium. Adv. Water Resour. (in press).

Kuppusamy, T., Sheng, J., Parker, J.C. and Lenhard, R.J., 1987. Finite element analysis of multiphase immiscible flow through soils. Water Resour. Res., 23: 625–632.

Lenhard, R.J. and Parker, J.C., 1987. Measurement and predictions of saturation–pressure relationships in three phase porous media systems. J. Contam. Hydrol., 1: 407–424.

Lyman, W.J., Reehl, W.F. and Rosenblatt, D.H., 1982. Handbook of Chemical Property Estimation Methods. McGraw-Hill, New York, NY, 335 pp.

Millington, R.J., 1959. Gas diffusion in porous media. Science, 130: 100–102.

Osborne, M. and Sykes, J., 1986. Numerical modeling of immiscible organic transport at the Hyde Park landfill. Water Resour. Res., 22: 25–33.

Parker, J.C. and Lenhard, R.J., 1990. Vertical integration of three phase flow equations for analysis of light hydrocarbon plume movement. Transp. Porous Media (in press).

Parker, J.C., Lenhard, R.J. and Kuppusamy, T., 1987. A parametric model for constitutive properties governing multiphase fluid flow in porous media. Water Resour. Res., 23: 618–624.

Parker, J.C., Kaluarachchi, J.J. and Katyal, A.K., 1988. Areal simulation of free product recovery from a gasoline storage tank leak site. Proc. Conf. on Petroleum Hydrocarbons and Organic Chemicals in Groundwater: Prevention, Detection and Restoration. N.W.W.A. (Natl. Water Well Assoc.), Houston, TX.

Reeves, H.W. and Abriola, L.M., 1988. A decoupled approach to the simulation of flow and transport of non-aqueous organic phase contaminants through porous media. Proc. 7th Int. Conf. on Computational Methods in Water Resources. M.I.T. (Mass. Inst. Technol.), Cambridge, MA.

Sleep, B.E. and Sykes, J.F., 1989. Modeling the transport of volatile organics in variably saturated media. Water Resour. Res., 25: 81–92.